Vertical mixing of commercial aviation emissions from cruise altitude to the surface

D. B. Whitt,[1] M. Z. Jacobson,[1] J. T. Wilkerson,[1] A. D. Naiman,[2] and S. K. Lele[2]

[1]   Data analysis and numerical simulations were used to examine vertical transport of cruise-altitude commercial aircraft emissions to the surface. First, aircraft emission data were compared with static stability and potential temperature data from satellites. Second, we ran global 3-D simulations of a passive tracer released uniformly at 11 km (cruise altitude). We present global, regional, and seasonal results of the data comparisons as well as approximate time scales of vertical mixing derived from the simulations. Using the year 2006 as a case study, we found that 24% of all global commercial aviation emissions occurred in the stratosphere, 17% occurred both north of 40° N and above the 330 K isentrope, and 54% occurred in regions of at least moderate static stability ($N^2 > 10^{-4}$ s^{-2}). In addition, 74% of emissions in the Arctic Circle were in the stratosphere. In the 3-D simulations, the globally averaged tracer-plume e-folding lifetime against vertical transport to any other altitude was 16 days during January and 14 days during July. Furthermore, the passive tracer took 15 days longer in January (77 days) compared with July (62 days) to achieve a surface-to-cruise mixing ratio fraction greater than 0.5 at all latitudes. The dynamical mixing time scales of extratropical cruise-altitude emissions were significantly longer than the globally averaged wet removal time of 4–5 days for aerosol particles emitted in the lower troposphere. Thus, it is unlikely that cruise-altitude emissions affect surface air quality via transport alone outside the tropics.

Citation: Whitt, D. B., M. Z. Jacobson, J. T. Wilkerson, A. D. Naiman, and S. K. Lele (2011), Vertical mixing of commercial aviation emissions from cruise altitude to the surface, *J. Geophys. Res.*, *116*, D14109, doi:10.1029/2010JD015532.

1.   Introduction

[2]   Commercial aviation is a steadily growing, energy intensive industry. The average annual growth rate in passenger traffic was 5.3% per year between 2000 and 2007 [*Lee et al.*, 2009], and the industry accounts for approximately 5.8% of all oil consumption world wide [*Mazraati*, 2010]. Consequently, it is important to identify potential impacts of aviation on climate and public health. Several previous studies have shown that aviation emissions may have a significant effect on global climate by adding emissions of greenhouse gases, changing the chemistry in the upper troposphere and lower stratosphere (UTLS) and changing global cloudiness (see *Lee et al.* [2009] for a review). Studies have also shown that emissions during landing and takeoff affect surface air quality [e.g., *Herndon et al.*, 2004; *Unal et al.*, 2005]. Several studies have modeled cruise-altitude emissions as a passive tracer [e.g., *Danilin et al.*, 1998; *Gettelman*, 1998; *Gettelman and Baughcum*, 1999]. Others have investigated the effects of aviation on the chemical composition of the troposphere using chemistry-transport models [e.g., *Brasseur et al.*, 1996; *Tarrason et al.*, 2004; *Köhler et al.*, 2008; *Barrett et al.*, 2010].

[3]   *Brasseur et al.* [1996] and *Köhler et al.* [2008], for example, observed that aviation caused increased levels of surface ozone. *Köhler et al.* [2008] went on to conclude that the elevated surface ozone must be due to vertical transport since the lower troposphere is a chemical sink for ozone.

[4]   However, only *Tarrason et al.* [2004] and *Barrett et al.* [2010] explicitly considered the impacts of cruise-altitude emissions on surface air quality and public health. *Barrett et al.* [2010] addressed the public health effects by modeling the premature mortality due to cruise-altitude emissions and found that the mortality impacts of cruise altitude emissions were due primarily to secondary aerosols. Furthermore, they found that cruise-level emissions account for about 80% of the premature mortality impact of aviation.

[5]   Although these studies raise some important concerns about aviation's effect on public health, the results from all four of these chemistry-transport studies must be interpreted with care because none of them considered aerosol-meteorology or aerosol-cloud feedbacks nor did any of these studies use a model with a particularly high vertical resolution in the UTLS (the vertical resolutions used in these four studies ranged from ~700–1000 m in the UTLS). In addition, these studies did not separate the transport from the other effects. In this study, we focus on the dynamical processes

---

[1]Department of Civil and Environmental Engineering, Stanford University, Stanford, California, USA.
[2]Department of Aeronautics and Astronautics, Stanford University, Stanford, California, USA.

which mix aviation emissions from cruise altitude to the surface and, in doing so, we begin to characterize the potential impact of cruise-altitude aircraft emissions on surface air quality via dynamical means.

[6] To that end, this paper presents and analyzes global commercial aviation emissions in tropopause relative (TR) coordinates and with respect to (1) potential temperature, (2) static stability, (3) the extratropical tropopause transition layer (ExTL), a chemically defined transition region described by *Hegglin et al.* [2009], and (4) the World Meteorological Organization (WMO) thermal tropopause height. Furthermore, the data are regionally and temporally disaggregated and statistics are reported.

[7] In addition, we present results from two idealized tracer release experiments run in a 3-D global computer model. The results of these experiments provide information about the vertical mixing time scales associated with an instantaneous tracer release at the peak of the vertical emissions distribution (11 km) during different seasons.

[8] Together, the data analysis and model results give important insights into this problem and serve as a starting point for a more accurate determination of the impact aviation has on surface air quality. However, to truly model the effects of aviation on surface air quality, a more complete modeling study must be undertaken which not only models the atmospheric dynamics and clouds, but also models the production and destruction of both emitted and secondary gaseous species as well as the transport, feedbacks, and removal of aerosols. This paper is a first step towards that goal.

2. Data Description

2.1. Emission Data

[9] Emission data were obtained from the Volpe National Transportation Systems Center and originally determined from the Federal Aviation Administration's Aviation Environmental Design Tool described by *Roof et al.* [2007]. For the purposes of this study, we viewed the emissions as a passive tracer in order to isolate the effects of dynamical processes. Consequently, we retained only the total fuel burn data rather than the array of constituent emissions.

[10] The data were binned into a 4-D matrix with daily temporal resolution and $1° \times 1° \times 100$ m (latitude $\times$ longitude $\times$ altitude) spatial resolution using the procedure described by *Wilkerson et al.* [2010]. The vertical coordinate was then transformed from a mean sea-level (MSL) relative to a mean TR coordinate in order to compare the emission data with background atmospheric properties of the UTLS, e.g., static stability or chemical composition, which are best presented in TR coordinates due to steep vertical gradients that move over time with the thermal tropopause [*Pan et al.*, 2004; *Hegglin et al.*, 2009; *Grise et al.*, 2010].

[11] An algorithm was applied to make this coordinate transformation [e.g., *Birner*, 2006]. The algorithm has the following steps. For each day and every horizontal location within the 4-D fuel-burn matrix, there exists a column vector of fuel burn data such that each element of the vector is a mass of fuel burned. The index of the element corresponds to the altitude above MSL (e.g., the nth element in the vector contains the emissions at $(n - 1) \times 100$ m above

MSL). Those emissions that occur between 7 and 13 km in MSL coordinates are moved to the element of the vector with the index corresponding to their TR height,

$$z_{TR} = z_{MSL} - z_{TH} + \overline{z_{TH}}, \tag{1}$$

[*Birner*, 2006] where z_{TH} is the tropopause height above MSL on that day and $\overline{z_{TH}}$ is the average tropopause height for the year. In this coordinate transformation, we do not move those emissions below 7 km because they are far below the tropopause and hence would remain in the troposphere independent of this transformation. In the final step, we reduce the horizontal resolution of the emission data to match that of the atmospheric data ($2° \times 20°$) described in detail in the next section.

2.2. Atmospheric Data

[12] In this section we define the background atmospheric properties used as metrics in this study.

[13] The height of the tropopause is defined throughout this paper, as specified by the WMO, as the "lowest level at which the temperature lapse rate decreases to 2 K km^{-1} or less and the lapse rate averaged between this level and any level within the next 2 km does not exceed 2 K km^{-1}" [*Holton et al.*, 1995].

[14] We used the gridded global $1° \times 1°$ level 3 tropopause height data product from the National Air and Space Administration (NASA) Atmospheric Infrared Sounder (AIRS) [e.g., *Parkinsin et al.*, 2003] to transform other 3-D atmospheric and emission fields into TR coordinates. Gores in the satellite data were filled by averaging the values of the day before and the day after. These 365 2-D (latitude $\times$ longitude) matrices of daily global tropopause heights, z_{TH}, were averaged to produce one 2-D matrix, $\overline{z_{TH}}$ (the global annually averaged tropopause height), for use in equation (1). Although there is some uncertainty in the AIRS daily tropopause height (~ 500 m), it is unlikely that this uncertainty will affect our results since it is not thought to be biased [*Olsen et al.*, 2007].

[15] Static stability is defined throughout this paper by the atmospheric Brunt-Väisälä frequency,

$$N^2 = \frac{g}{\theta} \frac{\partial \theta}{\partial z}, \tag{2}$$

where $g = 9.81$ m/s^2 is the gravitational acceleration, and

$$\theta = T \left(\frac{p_0}{p} \right)^\kappa, \tag{3}$$

is the potential temperature, where T is the temperature in Kelvin, $p_0 = 1000$ hPa is the standard reference pressure, p is the local air pressure and $\kappa = R/C_p \approx 2/7$ where R is the gas constant and C_p is the specific heat of dry air at constant pressure.

[16] The potential temperature and static stability data were derived from vertical temperature and pressure profiles at 100 m resolution that were obtained via GPS-radio occultation by the Challenging Minisatellite Payload (CHAMP) and the University Corporation for Atmospheric Research (UCAR) Constellation Observing System for Meteorology, Ionosphere, and Climate (COSMIC) [*Wickert et al.*, 2001;

Anthes et al., 2008]. Approximately 200 profiles are available per day from CHAMP and over 1000 profiles per day are available from COSMIC.

[17] For each vertical profile of temperature and pressure, the potential temperature was derived using equation (3) and the static stability was derived using equation (2). Then the local thermal tropopause height in each column, z_{TH}, was obtained using the algorithm described in the appendix of *Birner* [2006]. Finally, the static stability and potential temperature data in each column were transformed to TR coordinates as described in section 2.1. The mean tropopause height used in the transformation was obtained from the AIRS data described above.

[18] Unfortunately, because COSMIC data was only available in the second half of 2006, we were forced to use a rather coarse horizontal and temporal resolution of 2° × 20° × 1 month (latitude × longitude × time). This latitudinally biased resolution was chosen because potential temperature and static stability are significantly more variable along meridians than along circles of latitude [*Grise et al.*, 2010]. These data were further restricted to the atmosphere above 5 km where water vapor mixing ratios are lower and hence have less effect on atmospheric stability. Temperature profiles from GPS-radio occultation are also more accurate at higher altitudes than at lower altitudes [*Kursinski et al.*, 1996; *Grise et al.*, 2010].

[19] The ExTL was defined based on correlations of the mixing ratios of O_3, CO and H_2O in the UTLS obtained from the Atmospheric Chemistry Experiment Fourier Transform Spectrometer by *Hegglin et al.* [2009]. Furthermore, it was defined in a constant position relative to the tropopause based on the annual data provided by *Hegglin et al.* [2009, Figure 8]. Seasonal variability, except that which occurred as a result of the motion of the tropopause, was neglected.

3. Model Description

[20] In order to examine vertical transport and mixing of cruise-altitude emissions and determine the time scales associated with these processes, we ran simulations with the Gas, Aerosol, Transport, Radiation, General Circulation, Mesoscale, and Ocean Model (GATOR-GCMOM) [e.g., *Jacobson*, 2010]. This is a one-way-nested (feeding information from coarser to finer domains) global-regional computer model that simulates climate, weather, and air pollution on many scales. The model and its algorithms have been compared with gas, aerosol, radiative, meteorological, and surface data and numerical solutions in over 50 studies [e.g., *Zhang*, 2008; *Jacobson*, 2008, 2010; *Jacobson et al.*, 2011].

[21] In this study, the global model was run to examine the transport of an inert tracer initialized uniformly over the globe with a narrow Gaussian distribution in the vertical, centered at 11 km above sea level. The only processes affecting the tracer were atmospheric horizontal and vertical advection and diffusion based on online-predicted winds/ diffusion coefficients and vertical transport in subgrid convective clouds (which affected transport primarily in the tropics). The momentum equations on the global scale were solved with the potential-enstrophy, vorticity, energy, and mass-conserving scheme of *Arakawa and Lamb* [1981]. Horizontal and vertical advection of the tracer and water vapor

were solved with the mass-conserving, peak-preserving, mixing ratio bounded advection algorithm of *Walcek* [2000]. Eddy diffusion coefficients, used for a second-order local closure calculation of tracer diffusion, were calculated at all heights with the level 2.5 scheme of *Mellor and Yamada* [1982]. Cloud processes, including vertical transport of tracers in subgrid clouds, were simulated as described in section 2.4 of *Jacobson* [2010].

[22] The model was run over a global domain (4°-SN × 5°-WE resolution) with 89 sigma-pressure layers from the ground to ~60 km with 500 m vertical resolution from 1–21 km, 1 km resolution from 21–50 km, 2 km resolution from 50–60 km and fourteen layers in the bottom kilometer.

[23] Two experiments were performed. The first began 1 January 2006, and the second began 1 July 2006. Both were run for 150 days. The model was initialized with 1° × 1° reanalysis meteorological fields (1° × 1°, 2007, Global Forecast System, http://nomads.ncdc.noaa.gov/data/gfs-avn-hi/) and run forward in time with no data assimilation. The initial mixing ratio of the passive tracer peaked at 11 km above MSL and was initialized with the mixing ratio

$$M = 1000 \exp\left[-\left(\frac{z_{MSL} - 11}{0.5}\right)^2\right], \qquad (4)$$

where z_{MSL} was the altitude above sea level in kilometers and M was in units of ppbv. Although wet removal should be significant in the lower troposphere [*Schulz et al.*, 2006], all removal processes were turned off in these experiments in order to isolate the effects of dynamical transport and mixing. Therefore, our approach was different from that of *Danilin et al.* [1998], where 1992 emission data were modeled as a passive tracer but removed by a parameterized wet removal process at 7 km.

[24] We also compared modeled static stability with static-stability data derived from satellites. The procedure used to derive modeled static stability is slightly different from that used to derive the data-based results. Instead of using 3-D model output, we begin with daily and zonally averaged pressure and temperature at 4° × 568.2 m resolution. We then interpolate these outputs to approximately 100 m resolution. We find the tropopause height, z_{TH}, at every latitude and for each day from $\partial T/\partial z$, which is obtained via a fourth order central difference. Then we compute the monthly average tropopause height, $\bar{z}_{TH}$, by averaging the daily values. Finally, we derive the static stability using equation (2) and transform the results to TR coordinates using equation (1). We discuss the results of this comparison between model output and data in section 6.

4. Data Analysis Results

[25] Figure 1 shows two plots of the zonal sum of all global commercial aviation emissions and contours of the zonally averaged potential temperature and static stability in TR coordinates. Table 1 shows the associated statistics quantifying the emissions that occurred at different levels of potential temperature and static stability by both percentage and mass. Table 1 also separates the emissions with respect to the ExTL and the thermal tropopause.

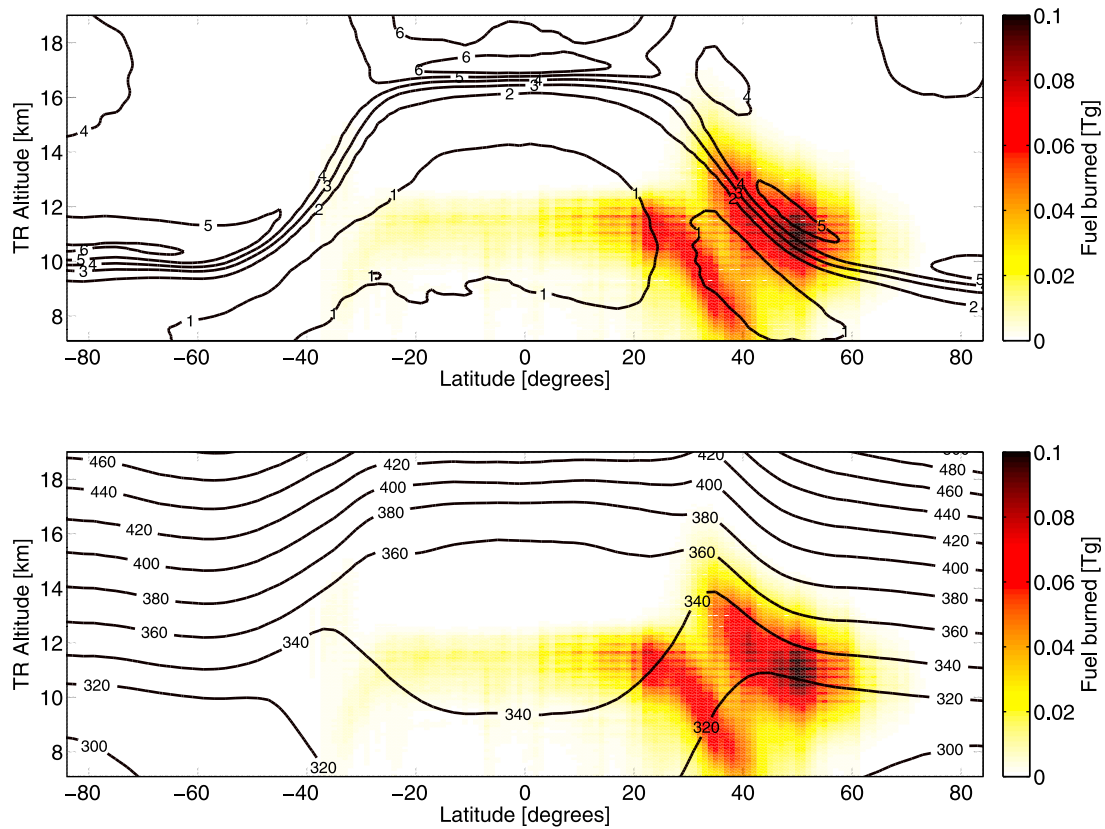[26] We find that a slightly greater percentage of commercial aviation emissions were deposited into the strato-

Figure 1. Jet fuel burned by commercial aircraft in the year 2006 as a function of latitude (degrees) and TR altitude (km). We consider all latitudes, from 90°S to 90°N. However, we only consider TR altitudes from 7 to 19 km, where the TR altitude is defined by equation (1). In both of these plots, the fuel burn is zonally and annually summed. The dark lines are contours of (top) static stability (N^2) defined by equation (2) and (bottom) potential temperature (θ) defined by equation (3). Both N^2 and θ are derived from CHAMP and COSMIC data as described in section 2.2 and zonally and annually averaged.

Table 1. Commercial Aviation Fuel Burned Globally in the Year 2006 Disaggregated by Background Atmospheric Properties[a]

Fuel Burned (Tg)	Percent	Category
45.6	24	stratosphere
143	76	troposphere
13.3	7	$315K > \theta > 300K$
46.3	25	$330K > \theta > 315K$
49.7	26	$345K > \theta > 330K$
28.2	15	$360K > \theta > 345K$
7.45	5.2	$\theta > 360K$
61.5	33	in ExTL
4.62	2.5	above ExTL
46.5	25	$N^2 < 1\ E\text{-}4\ s^{-2}$
51.9	28	$2E\text{-}4s^{-2} > N^2 > 1\ E\text{-}4\ s^{-2}$
46.7	25	$N^2 > 2\ E\text{-}4\ s^{-2}$
188	100	2006 Total

[a]We disaggregate the commercial aviation fuel burned globally in the year 2006 by background atmospheric properties including the location relative to the thermal tropopause, the location relative to the ExTL, the background potential temperature (θ) and the background static stability (N^2). In the case of the ExTL, potential temperature and static stability, only the fuel that was burned above 5 km in tropopause relative coordinates is considered (78% of the total). Hence, the sum of these particular disaggregations should not add to 100%. Note that only commercial aviation emissions were included in this study. Military and general civil aviation were not included and could account for as much as 20% more fuel burned during the year [*Lee et al.*, 2009].

sphere in 2006 (24%) compared with 1992 (20%). This difference could have been caused by a variety of factors. Between 1992 and 2006, flight patterns may have changed, more accurate information about flight paths may have become available, and the tropopause may have been slightly lower on average. Some results from these two inventories are compared in Table 2.

4.1. Spatial Disaggregation

[27] As Figure 1 illustrates, the emissions trend toward higher potential temperatures and more stable air with

Table 2. Comparison of a 1992 Emissions Inventory With the 2006 Inventory Used in Our Study[a]

Percent of 2006	Percent of 1992	Category
76	80	below thermal tropopause
67	70	below tropopause minus 1 km
62	61	below tropopause minus 2 km

[a]This table compares a 1992 emissions inventory with the 2006 inventory used in our study. Commercial aircraft burned 35% more fuel in 2006 (188 Tg) than in 1992 (139 Tg). Furthermore, 4% more jet fuel was burned in the stratosphere in 2006. The 1992 results are described by *Gettelman and Baughcum* [1999], and the 2006 results are described in sections 2.1 and 2.2 of this paper. The comparison is made based on the location of the fuel burned relative to the thermal tropopause height, which is obtained from reanalysis data in 1992 and satellite data in 2006.

Table 3. Fuel Burned in 2006 in the Extratropical Northern Hemisphere and the Arctic Circle[a]

Percent of AC	Percent of ExTNH	Category
74	47	stratosphere
26	53	troposphere
31	13	$315 > \theta > 300K$
28	28	$330K > \theta > 315K$
22	17	$345K > \theta > 330K$
10	13	$360K > \theta > 345K$
2.9	7.9	$\theta > 360K$
91	58.7	in ExTL
1.0	4.4	above ExTL
2.0	11	$N^2 < 1 \text{ E-4 } s^{-2}$
15	20	$2E\text{-}4 \ s^{-2} > N^2 > 1E - 4s^{-2}$
79	49	$N^2 > 2 \text{ E-4 } s^{-2}$

[a]Of the 188 Tg of fuel burned in 2006, 82.8 Tg were burned in the extratropical Northern Hemisphere (ExTNH), between 40°N and 90°N, and 2.35 Tg were burned in the Arctic Circle (AC), between 66.56°N and 90°N. We disaggregate the commercial aviation fuel burned in these regions during 2006 by background atmospheric properties including the location relative to the thermal tropopause, the location relative to the ExTL, the background potential temperature (θ) and the background static stability (N^2). In the case of the ExTL, potential temperature, and static stability, only the fuel that was burned above 5 km in tropopause relative coordinates is considered. Hence, the sum of these particular disaggregations should not add to 100%.

increasing latitude. This fact can be confirmed by examining regional statistics in Table 3, which contains the emissions that occur in the extratropics (latitude >40°N) and the Arctic Circle (latitude >66.56°N). Although the results are, perhaps, intuitively obvious, they are important because they suggest a qualitative description of the mixing processes relevant to all those emissions which occur in the extratropics, near and above the tropopause and in regions of moderate or high static stability (~one third of the total) which we now describe in more detail.

[28] The dominant dynamical mixing process relevant to the near-tropopause emissions is quasi-isentropic horizontal eddy mixing, with time scales of days, punctuated by fairly vigorous but highly episodic and localized vertical mixing in subtropics and midlatitudes with time scales of hours to days [e.g., *Holton et al.*, 1995; *Gettelman and Sobel*, 2000; *Hoor et al.*, 2010]. These vertical mixing events are due to a variety of different processes including, for example, isentropic stratosphere-to-troposphere transport in the subtropics followed by convection in the troposphere, deep stratospheric intrusions, and midlatitude storm systems [e.g., *Shapiro*, 1980; *Holton et al.*, 1995; *Stohl et al.*, 2003b]. Although stratosphere-troposphere exchange (STE) is not completely understood, the net downward movement via diabatic processes is thought to be controlled primarily from above by internal wave breaking in the stratosphere [*Haynes et al.*, 1991]. Hence, although there may be a few rather strong localized STE events which could dramatically impact surface air quality in a small region over a short time, the long-time averaged subsidence which operates on time scales of months to years should theoretically have a limited effect on surface air quality [*Brewer*, 1949].

[29] A variety of references are available that describe and illustrate the spatial structure of the mixing and transport processes in more detail. Figures 13.17 and 13.18 of *Vallis* [2006] as well as several figures in *Pierrehumbert and Yang* [1992] illustrate the chaotic horizontal eddy stirring and mixing which dominate the horizontal transport of aviation emissions. *Huber et al.* [2000] and *Haynes and Shuckburgh* [2000] show climatological information about turbulent horizontal eddy diffusion. *Stohl et al.* [2003b, Figure 1] diagram the vertical processes involved and their typical latitudes. *Gettelman and Sobel* [2000, Figure 5] and *Hoor et al.* [2010, Figure 2] give a more thorough depiction of the typical horizontal locations of the rapid STE processes. These processes are hard to describe in an average sense because their occurrence is typically related to chaotic geostrophic turbulence. Nevertheless, the distribution of STE events does have a relatively robust zonal structure on average [e.g., *Chen*, 1995; *Gettelman and Sobel*, 2000; *Hoor et al.*, 2010].

4.2. Temporal Disaggregation

[30] Since only annual data are presented in Figure 1, the marked seasonal variability may not be immediately apparent. Nevertheless, our data analysis confirms that of *Gettelman* [1998] which showed marked seasonal variability in the data. The two most important seasonal differences of consequence to aviation emissions are: (1) the increased height of the Northern Hemisphere (NH) summer subtropical and midlatitude tropopause and, (2) the reduced strength of the NH summer subtropical jet. Figure 2 compares the zonal mean tropopause heights in January and July 2006, and *Marshall and Plumb* [2008, Figure 5.20] show the mean zonal wind during the summer and the winter. Both of these seasonal differences can lead to enhanced vertical mixing of aviation emissions in July as described below.

[31] In the first case, the upward shift in the tropopause means that aviation emissions, which occur at roughly the same altitudes throughout the year, tend to occur more frequently in the troposphere and regions of reduced static stability in the summer compared with the winter. In fact, we found that 33% of January 2006 commercial aviation emissions occurred in the stratosphere whereas only 13% of July 2006 emissions occurred there. These results are similar to results obtained by *Gettelman* [1998] despite the fact that our study used a thermal tropopause definition and *Gettelman* [1998] used a dynamic definition. As one might expect, the seasonal pattern was found to be roughly the same, regardless of the choice of tropopause definition, although the magnitudes of the values are different. In this study, we retain only the thermal definition, despite the issues associated with using it in a dynamical study, because we would like to base this data analysis part of our study entirely on data rather than assimilated model results which would be required to define a potential vorticity.

[32] In the second case, the reduced intensity of the subtropical jet leads to increased effective horizontal eddy diffusivity along those isentropic surfaces between 330K and 380K during the summer [*Haynes and Shuckburgh*, 2000]. Consequently, summer STE along isentropic surfaces might be enhanced. That said, the picture of stronger summer STE is complicated by the fact that the frequency of deep tropospheric intrusions associated with midlatitude storm systems peaks in the winter [*Stohl et al.*, 2003a]. This trend was also seen in the results of *Gettelman* [1998] where STE was enhanced during the summer in the subtropics and enhanced during the winter in the midlatitudes. Understanding the net effect of STE on aviation emissions is further complicated
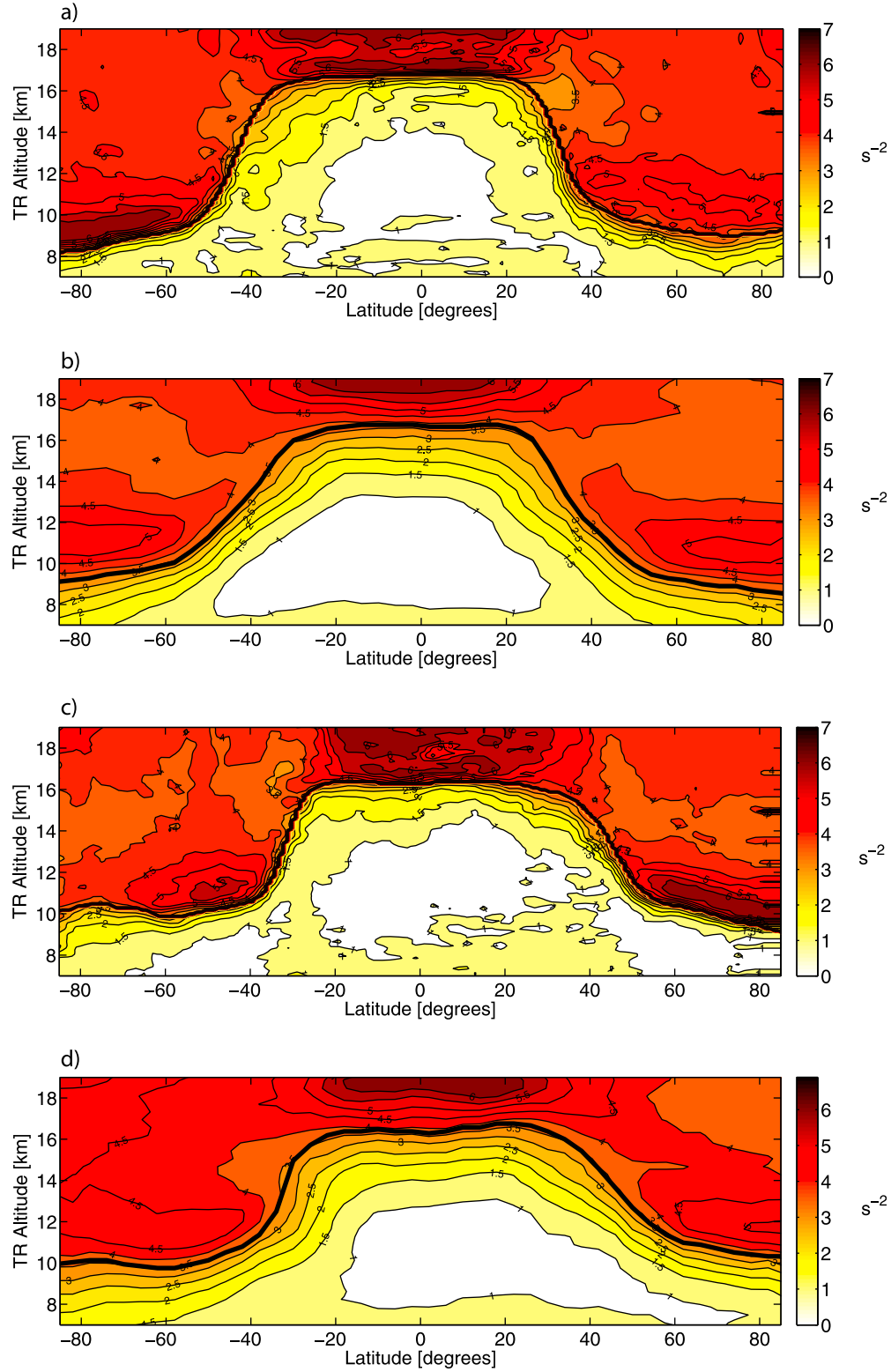
Figure 2. These four plots compare (b and d) GATOR-GCMOM results with (a and c) satellite data. The months of January (Figures 2a and 2b) and July (Figures 2c and 2d) 2006 are considered. In each case, we plot the zonally and monthly averaged static stability (N^2) as a function of latitude (degrees) and TR altitude (km). The axes are the same as in Figure 1. The black lines mark the zonally and monthly averaged tropopause heights.
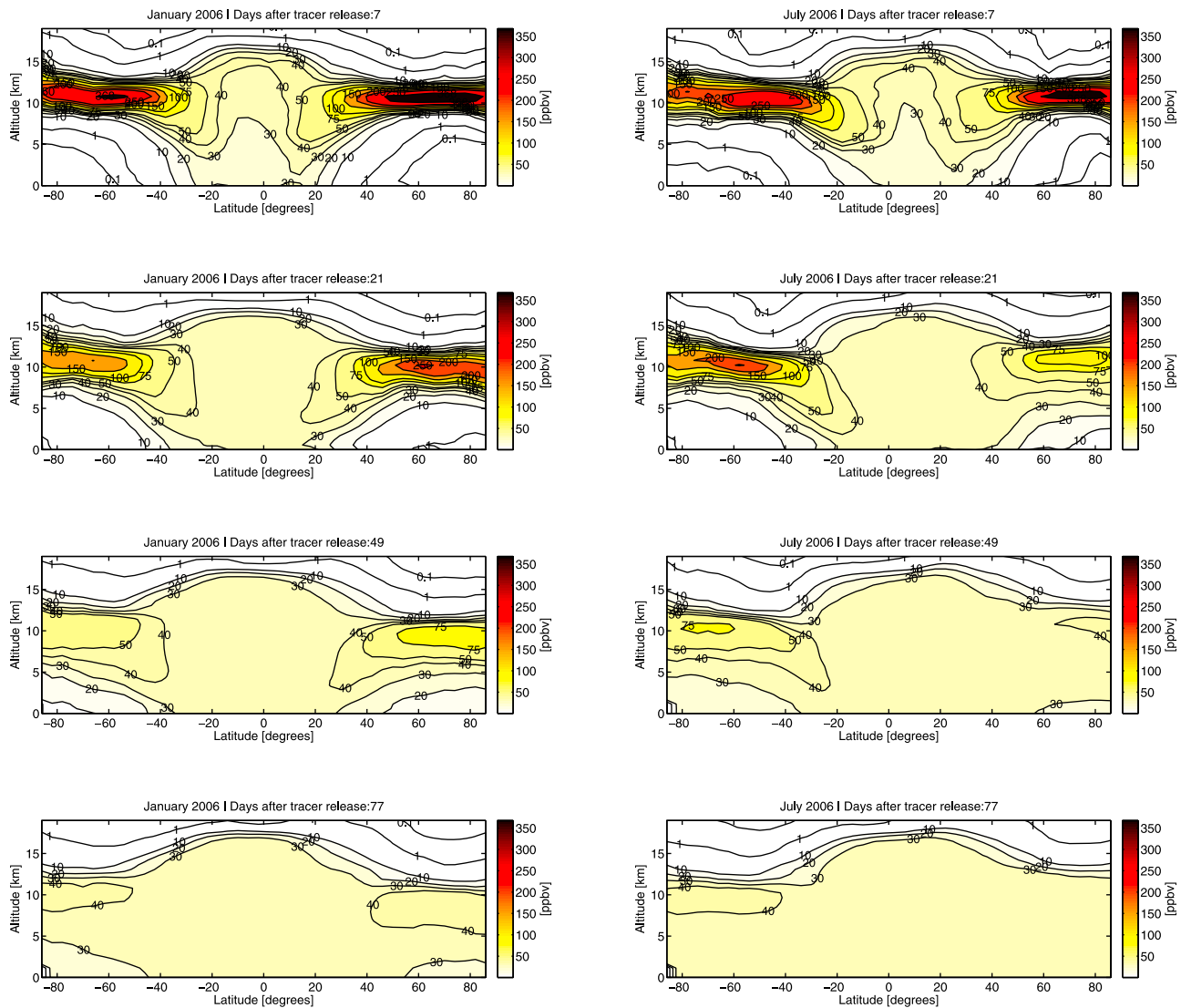
Figure 3. Eight snapshots of the tracer mixing ratios derived from GATOR-GCMOM, (left) four from the simulation beginning in January and (right) four from the simulation beginning in July. The results are plotted as a function of latitude (degrees) and MSL altitude (km) (from 0 to 20 km). We consider the following 4 days after the tracer release: (top to bottom) 7, 21, 49, and 77 days. The tracer mixing ratios are zonally and daily averaged values.

by the fact that STE is neither unidirectional nor symmetric. For example, *Gettelman* [1998] found that although more emissions occurred in the troposphere during July, a significant fraction of these emissions were then lofted into the stratosphere from the tropics and subtropics making the net stratospheric mass fraction of emissions after a 30 day adjustment period similar in January (13%) and July (15%). Therefore, it is important to be careful when drawing conclusions about the seasonal variation in vertical mixing of aviation emissions.

5. Model Results

[33] Figures 3 and 4 illustrate the results of a passive tracer release simulated in GATOR-GCMOM as described in section 3. Strong vertical mixing in the tropics occurred primarily due to the vertical transport of the tracer in subgrid convective clouds and to the weaker static stability in that region, as illustrated in Figure 2. Complete tropospheric mixing of the pulse inert tracer (no wet or dry removal, no chemistry) from 11 km was faster in July than January (see, e.g., day 77 of Figure 3).

[34] Although mixing was faster in July, the two simulations were more similar than different. We observe in Figure 4 that the surface tracer mixing ratios averaged over the first month were low everywhere outside the tropics except in regions of very high topography. We also observe in Figures 3 and 4 that mixing was slower in the winter hemisphere in both simulations because the tropical tropopause had shifted towards the summer hemisphere as shown in Figure 2. Therefore, the tracer was released into stable air in a larger latitude range in the winter hemisphere. Furthermore, Figure 5
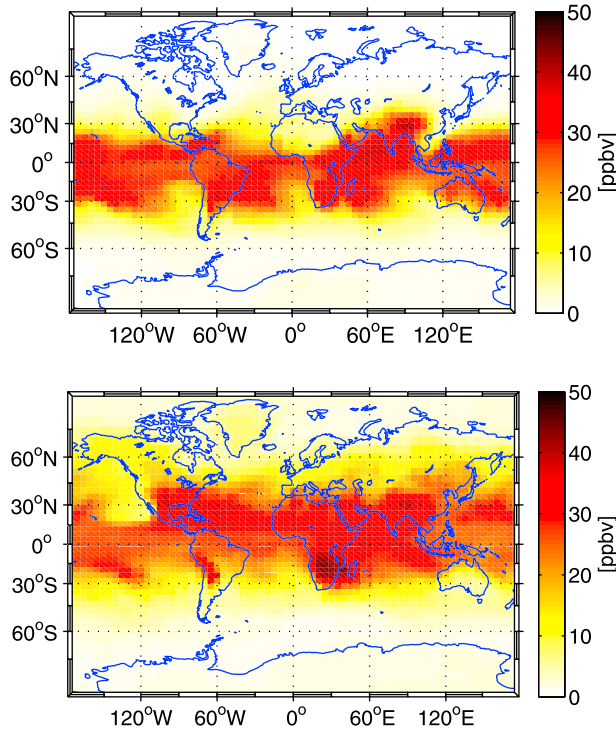
Figure 4. The (top) January and (bottom) July average surface tracer mixing ratio. We observe that the mixing ratios were low outside the tropics except in regions of very high topography during the first month of each simulation. However, in July, when the tropical belt shifted north, the tracer came down in populated NH regions more rapidly.

confirms that, in both simulations, the respective winter subtropical jet was stronger than the respective summer subtropical jet. Hence, the effective horizontal eddy diffusivity was lower and the mixing via quasi-isentropic horizontal transport to regions of higher convection was slower in the winter hemisphere.

[35] However, as a consequence of topography, the NH subtropical jet was weaker in the boreal summer (July) than the Southern Hemisphere (SH) jet was in the austral summer (January) so the mixing times were not symmetric in the two simulations. For similar reasons, the SH jet in the austral winter (July) was stronger than the NH jet in the boreal winter (January). These observations do not necessarily suggest that one simulation should see more rapid globally averaged vertical mixing. The model results, however, did show that globally averaged mixing was faster in July. The most likely explanation for this result is that the extratropical tropopause was on average 1.0 km higher in July (11.0 km outside 34°S–34°N) than in January (10.0 km outside 34°S–34°N). This observation is consistent with a climatological pattern of higher globally averaged tropopause heights during the boreal summer which has been observed in reanalysis data (e.g., L. J. Wilcox et al., A global blended tropopause based on era data. Part I: Climatology, submitted to the *Quarterly Journal of the Royal Meteorological Society*, 2011). Nevertheless, these results benefit from further quantification and analysis.

[36] We quantify the seasonal differences in two ways. First we define the "surface-to-cruise mixing ratio fraction" at every latitude,

$$MRF = \frac{MR_{\text{surface}}}{MR_{\text{cruise}}}, \qquad (5)$$

where MR_{surface} is the mixing ratio at the surface, initially 0 ppbv, and MR_{cruise} is the mixing ratio at the altitude above MSL where the zonally averaged vertical distribution of the tracer mixing ratio is at a peak. We found that this altitude associated with the zonally averaged peak mixing ratio descended at a rate of about 500 m to 1000 m per month in the extratropics before the plume was well mixed because of the slow subsidence associated with the Brewer-Dobson circulation.

[37] A time series of MRF over all latitudes was obtained for both simulations and is plotted in Figure 6. We found that it took 15 days longer for MRF to reach values greater than 0.5 at all latitudes in January compared with July. Although it makes sense that summer mixing should be faster in the NH in July than in the SH in January because of the relative strength of the subtropical jets, it is not obvious why complete tropospheric mixing should be faster during austral winter than during austral summer in the SH as shown in Figure 6. The reasons for this result are not obvious but the root cause was most likely the height of the tropopause. We observed that the austral winter tropopause was actually higher in the SH than it was in the austral summer by roughly 1 km as mentioned above (see Figure 2). As a result, the peak of the tracer distribution was much closer to the tropopause in the winter (less than 1 km ~1–2 grid cells). Consequently, more tracer was released into less stable tropospheric air during July in the SH than during January in the SH. The differences in static stability at 11 km and tropopause height relative to 11 km between the two simulations can be seen in Figure 7.

[38] Also shown in Figure 7 is the e-folding lifetime, τ, of the tracer at cruise altitude against vertical transport and mixing to any other altitude. This metric provides a different perspective on vertical mixing at cruise altitude than the MRF and helps to further illustrate the subtleties involved in the dynamics. We define this e-folding lifetime at each latitude by assuming an exponential decay model for the mixing ratio at the peak of the vertical tracer distribution

$$MR_{\text{cruise}}(t) = MR_{\text{cruise}}(t_0)e^{-\frac{t}{\tau}}, \qquad (6)$$

where $MR_{\text{cruise}}(t_0)$ is the mixing ratio in the tracer plume averaged over the first day of the simulation and $MR_{\text{cruise}}(t)$ models the tracer mixing ratio in the plume as a function of time. We use an average over the first day as an initial value to minimize the impact of some unphysical model noise occurring at startup. Furthermore, we fit the e-folding lifetime to the first two e-folding periods to provide more representative results in the extratropics. More specifically, using GATOR-GCMOM output, we find the time τ^1 when $MR_{\text{cruise}}(\tau^1)/MR_{\text{cruise}}(t_0) = e^{-1}$ and the time τ^2 when $MR_{\text{cruise}}(\tau^2)/MR_{\text{cruise}}(t_0) = e^{-2}$. We define $\tau = 0.5\tau^1 +$
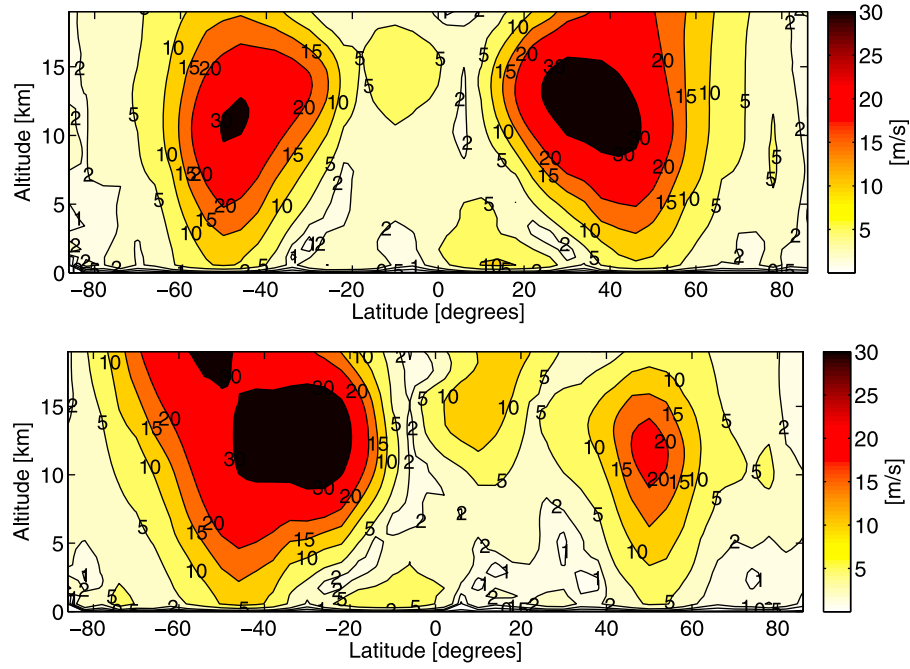
Figure 5. The (top) January and (bottom) July zonally averaged zonal wind from GATOR-GCMOM. We observe that, as we would expect, the NH subtropical jet is weaker in the boreal summer (July) compared with the SH subtropical jet in the austral summer (January). This would suggest greater quasi-isentropic STE in the boreal summer NH than the austral summer SH as seen in Figures 3, 6, and 7 and hence more rapid overall mixing in the July simulation. However, the results can not be reduced to this effect alone. The mixing is actually faster in the SH in July (austral winter), despite the reduced quasi-isentropic STE. The reasons for this are discussed in more detail in section 5.
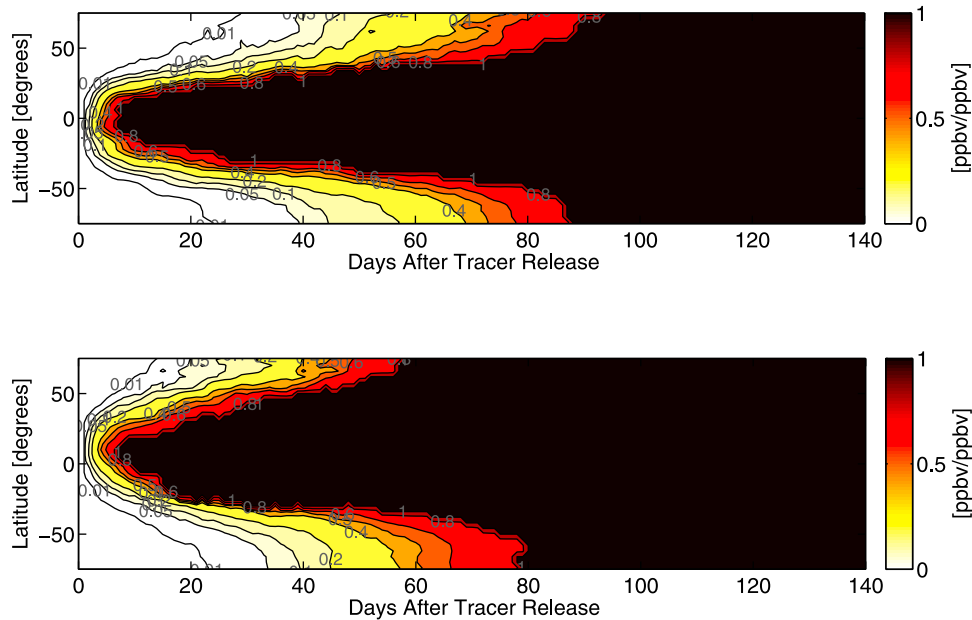

Figure 6. These two plots show the surface-to-cruise mixing ratio fraction (*MRF*), defined by equation (5), as a function of the simulation day and latitude (degrees), obtained from the (top) January simulation and (bottom) July simulation. Once $|MR_{cruise} - MR_{surface}| < 10$ ppbv we set the $MRF = 1$ because it is no longer meaningful at such small mixing ratio gradients.
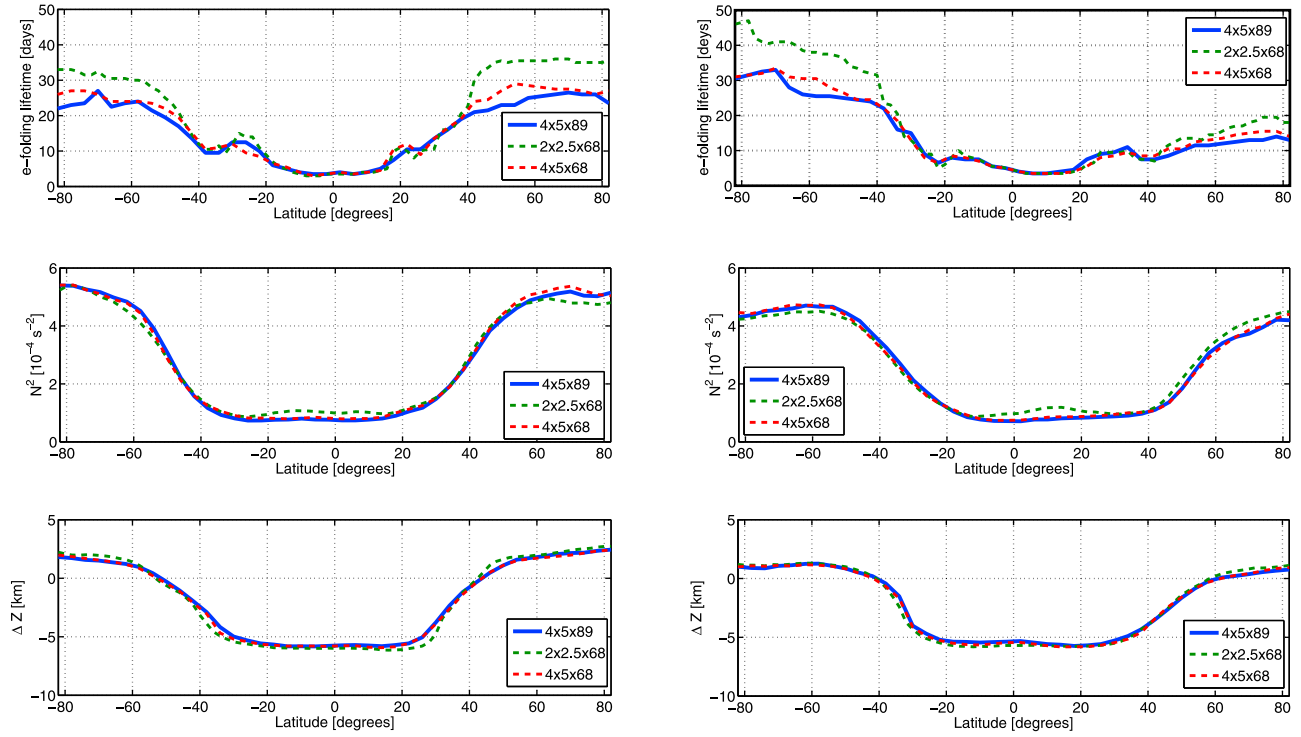
Figure 7. These six plots compare the (left) January and (right) July (top) e-folding lifetimes of the tracer plume (τ defined in equation (6)), (middle) static stability at 11 km, and (bottom) height of the tropopause compared to 11 km (i.e., $11 - \overline{z_{TH}}$). We see that longer e-folding lifetimes at 11 km roughly correlate with higher static stability at 11 km and greater distances above the tropopause. These plots show results from three different model resolutions. The solid line, $4 \times 5 \times 89$, denotes the simulations described in section 3 of this study. The dashed line $4 \times 5 \times 68$ denotes a simulation with similar initial conditions but a lower vertical resolution outside the region from 1 to 21 km. The dashed line denoted $2 \times 2.5 \times 68$ denotes a case with similar initial conditions but $2° \times 2.5°$ horizontal resolution and lower vertical resolution outside 1 to 21 km. The three simulations show consistent results.

$0.5(\tau^2 - \tau^1)$. Furthermore, if $|MR_{\text{cruise}} - MR_{\text{surface}}| < 10$ before $MR_{\text{cruise}}(\tau^2)/MR_{\text{cruise}}(t_0) = e^{-2}$, we set τ^2 equal to the first time when $|MR_{\text{cruise}} - MR_{\text{surface}}| < 10$. This change only affects the tropics where the cruise level mixing ratios averaged over the first day dropped below 250 ppbv.

[39] We found that the e-folding lifetimes peaked at higher latitudes where the tracer was released in the lowermost stratosphere. Figure 7 shows that higher e-folding lifetimes roughly correlated with higher values of static stability and lower tropopause heights. We also found that even though complete tropospheric mixing, as determined with *MRF*, was faster in SH austral winter than the SH austral summer, the e-folding lifetime of the SH plume was actually longer in austral winter. In this case, the two metrics told apparently opposing stories. However, it is important to note, that, as Figures 6 and 7 show, the differences between the mixing in the SH winter and the SH summer, as described by either metric, were not very large. Therefore, the only reasonable conclusion is that mixing from 11 km to the surface has similar timescales during the winter and summer in the extratropical SH.

6. Discussion of Model Results

[40] We now discuss our modeling results. In particular, we consider if our results are consistent with the results of earlier studies, we discuss metrics for studying tropospheric mixing time and we consider the effects of model grid resolution in our study.

[41] To our knowledge, no one has used the same definitions or experimental setup we use here to quantify mixing times from cruise altitude. However, our results are mostly consistent with the results of earlier studies. For example, *Liang et al.* [2009] prescribed seasonal cycles of stratospheric mixing ratios of several tracers with tropospheric lifetimes ranging from one to six months and used a chemistry-transport model to examine the evolution of the mixing ratios at various heights in the troposphere. They concluded that the average extratropical stratosphere-to-lowertroposphere transport time was about three months and that the transport time from the lower stratosphere to the upper troposphere was about one month based on modeled delays in the seasonal cycle of the mixing ratios at various altitudes. Using the *MRF* metric, we found that the complete tropospheric mixing time of a tracer released uniformly at 11 km was also approximately 3 months.

[42] *Forster et al.* [2003] and *Gettelman* [1998] both reported e-folding lifetimes of the mass aviation emissions in the stratosphere. Their definitions are different from our plume e-folding lifetime but their results add context to ours. *Forster et al.* [2003] found that the average e-folding lifetime of the mass of aviation emissions deposited in the

stratosphere in the North Atlantic Flight Corridor was 23 days. This number is significantly lower than the global averages found by *Gettelman* [1998] (~50 days). However, as *Forster et al.* [2003] pointed out, they used a slightly different definition of the e-folding lifetime than *Gettelman* [1998]. *Forster et al.* [2003] only considered those emissions which began in the stratosphere and remained there. They did not allow for any troposphere-to-stratosphere transport of emissions. Since STE is bidirectional and emissions occur in relatively large quantity both above and below the tropopause it makes sense that *Forster et al.* [2003] report a shorter e-folding lifetime.

[43] We emphasize again that our definition of e-folding lifetime is different from that of either *Gettelman* [1998] or *Forster et al.* [2003]. Our definition is based on the volumetric mixing ratio in the tracer plume whereas these two studies defined the e-folding lifetime based on the fraction of the total mass of emissions in the stratosphere. Nevertheless, we note that their results are basically consistent with our results and those of *Liang et al.* [2009]. Moreover, they support our thesis that extratropical cruise-altitude aviation emissions will not affect surface air quality via dynamical mixing alone.

[44] As the previous discussion highlights, the choice of metrics in a study such as this can be very important. In order to elucidate the physics, we present two metrics in this paper. However, even though the e-folding lifetime and the *MRF* tell similar stories about the physics we saw in our model runs, the *MRF* is a better metric to use when analyzing the effects of cruise-altitude emissions on surface air quality since it specifically incorporates the tracer mixing ratio at the surface. Nevertheless, there are still difficulties when comparing *MRF* with the lifetime of aerosol particles in the lower troposphere which is only 4–5 days, primarily due to wet removal [*Schulz et al.*, 2006; *Jacobson*, 2010]. In particular, the tracer in our experiments was emitted in the UTLS not the lower troposphere. Even with wet removal, aerosol particles emitted in the UTLS would have longer lifetimes than 4–5 days on average because there is less wet removal in the upper troposphere than in the lower troposphere. Furthermore, wet removal often occurs in convective systems which are also characterized by rapid vertical transport processes. Hence, vertical mixing time scales and wet removal rates can be locally coupled. The issue is further complicated by the fact that wet removal rates are not horizontally uniform. Nevertheless, only in the tropics, where dynamical mixing was rapid due to subgrid convective processes, did we find $MRF > 0.5$ in less than a week and in the extratropics the timescales of mixing were roughly an order of magnitude longer. This means that horizontal transport and mixing should be important for the extratropical cruise-altitude aviation emissions. Therefore, it is unlikely that these emissions would remain in regions of locally low wet removal for their entire lifetime in the troposphere. Therefore, one would expect that, on average, the effects of wet removal would dominate the effects of dynamical vertical mixing of extratropical cruise-altitude aviation emissions.

[45] One may still wonder, however, how the relevant model physics compare with the physics of the real atmosphere. To address this concern, we converted the daily and zonally averaged GATOR-GCMOM output into TR coordinates as described in section 3 and compared these results with our TR static stability data derived from the CHAMP and COSMIC satellites as described in section 2.2. Figure 2 contains plots of the January and July zonally averaged static stability for both the model output and the data. Although this is merely a qualitative comparison, we are pleased to see that the model captured much of the physics, including an accurately placed and relatively sharp tropopause along with a tropopause inversion layer.

[46] However, the model did not give a good representation without careful selection of the vertical resolution. In fact, our experiments with a lower resolution not reported here demonstrated the importance of a high vertical resolution in the UTLS. We saw great improvements when comparing the model- and data-derived tropopause heights and static stability (shown in Figure 2) after increasing our resolution in the region between 13 and 21 km from 1 km to 500 m. Like *Roeckner et al.* [2010], we saw that the tropopause was spuriously high with the lower vertical resolution in this region. On the other hand, increasing the horizontal resolution to $2° \times 2.5°$ which significantly increased the computational cost, did not prove to be as important on this test after increasing the vertical resolution.

[47] To illustrate some of the effects of grid resolution on our results, we compare, in Figure 7, some results from six simulations with similar initial conditions but different resolutions. We compare the two simulations described in section 3 of this paper with two simulations with higher horizontal resolution but lower vertical resolution and two simulations with the same horizontal resolution but lower vertical resolution (one for each season at each resolution). All of the simulations, however, have 500 m vertical resolution from 1 to 21 km. The differences are in the bottom kilometer and the stratosphere. The results are mostly consistent. Slightly higher extratropical tracer e-folding lifetimes at the higher horizontal resolution were likely due to reduced horizontal numerical diffusion which could cause horizontal mixing from the extratropics to the tropics and subsequent vertical mixing via convection. Although these plots do not conclusively illustrate the effects of grid resolution or the uncertainty in our results, they support our thesis and suggest that increases in horizontal resolution should only act to increase tropospheric mixing times.

[48] In this paper, we present results from a $4° \times 5°$ horizontal resolution with 500 m vertical resolution throughout the UTLS primarily because the model appears to adequately capture much of the physics at this resolution as discussed above. As in all numerical modeling, one must choose an optimal resolution based on competing interests. For this study, we prioritized minimizing vertical numerical diffusion over minimizing horizontal numerical diffusion, given the computational costs associated with each and the importance of these quantities when modeling the vertical mixing of a tracer plume from the lower stratosphere to the surface at higher latitudes (>40°). Although these idealized simulations are not too computationally intensive, minimizing computational cost will be important when attempting to use the full functionality of GATOR-GCMOM to model the effects of aviation emissions on climate and air quality

over longer time scales with online gas and aerosol chemistry in addition to clouds and dynamics.

7. Conclusions

[49] Before making conclusions, it is important to emphasize that this paper is just a first step toward understanding the effects of cruise-altitude emissions on surface air quality. The numerical experiments presented in this paper were idealized. We neglected chemistry and removal processes in order to isolate the effects of dynamical mixing. Nevertheless, many subgrid processes, including vertical mixing via cloud processes, were included [e.g., *Jacobson*, 2010] and the model has been shown to accurately describe important physical properties of the UTLS both here (e.g., Figure 2) and in previous studies [e.g., *Jacobson*, 2008]. With these thoughts in mind, we discuss the implications of our results.

[50] We see that the expected tropospheric lifetimes of many of the constituents of aviation emissions are quite a bit shorter than average tropospheric mixing time determined in this study. For example, as already mentioned, wet removal acts on time scales of, on average, 4–5 days in the lower troposphere [*Schulz et al.*, 2006; *Jacobson*, 2010]. The average lifetimes of the gaseous oxides of nitrogen are 1–4 days in the troposphere [*Seinfeld and Pandis*, 1998]. Even tropospheric ozone, which is not a direct emission but is produced as a secondary species above 5 km from aviation emissions [*Brasseur et al.*, 1996; *Köhler et al.*, 2008], has an average chemical lifetime of only 22 days [*Stevenson et al.*, 2006], which is roughly a factor of 4 shorter than the time scale for complete tropospheric mixing of a tracer emitted at 11 km. That said, it is important to observe that wet removal and ozone destruction both only work efficiently in the lower troposphere. Hence, the time scales are not perfectly comparable. Nevertheless, our mixing time scales are relatively robust and slow. Small changes in the dynamical mixing time scales due to improved model resolution would not be expected to significantly change the story. Extratropical surface air quality is unlikely to be affected by cruise-altitude aviation emissions via dynamical transport and mixing alone.

[51] We have shown that more than half of commercial aviation emissions occur in relatively stable regions of the atmosphere and that nearly one quarter occur in the stratosphere. Furthermore, we have shown that dynamical mixing time scales relevant to cruise-altitude emissions in the extratropics are significantly slower than several other relevant time scales. Our results highlight the importance of considering aviation emissions in context of the UTLS dynamics and, consequently, the importance of a high vertical resolution throughout the entire UTLS region when using global 3-D numerical models. Furthermore, we have shown that it is unlikely that extratropical cruise-altitude aviation emissions will affect surface air quality in an average sense via dynamical transport and mixing alone. On the other hand, we have not considered the effects of the numerous intense but localized events that make up the average behavior. More analysis is needed to determine the short term local effects of commercial aviation on surface air quality.

References

Anthes, R., et al. (2008), The COSMIC/FORMOSAT-3 mission: Early results, *Bull. Am. Meteorol. Soc.*, *89*, 313–333.

Arakawa, A., and V. R. Lamb (1981), A potential enstrophy and energy conserving scheme for the shallow water equations, *Monthly Weather Rev.*, *109*, 18–36.

Barrett, S. R. H., R. E. Britter, and I. A. Waitz (2010), Global mortality attributable to aircraft cruise emissions, *Environ. Sci. Technol.*, *44*, 7736–7742.

Birner, T. (2006), Fine-scale structure of the extratropical tropopause region, *J. Geophys. Res.*, *111*, D04104, doi:10.1029/2005JD006301.

Brasseur, G. P., J.-F. Müller, and C. Granier (1996), Atmospheric impact of NOx emissions by subsonic aircraft: A three-dimensional model study, *J. Geophys. Res.*, *101*, 1423–1428.

Brewer, A. M. (1949), Evidence for a world circulation provided by the measurements of helium and water vapor distribution in the stratosphere, *Q. J. R. Meteorol. Soc.*, *75*, 351–363.

Chen, P. (1995), Isentropic cross tropopause mass exchange in the extratropics, *J. Geophys. Res.*, *100*, 16,661–16,673.

Danilin, M. Y., et al. (1998), Aviation fuel tracer simulation: Model intercomparison and implications, *Geophys. Res. Lett.*, *25*, 3947–3950.

Forster, C., A. Stohl, P. James, and V. Thouret (2003), The residence times of aircraft emissions in the stratosphere using a mean emission inventory and emissions along actual flight tracks, *J. Geophys. Res.*, *108*(D12), 8524, doi:10.1029/2002JD002515.

Gettelman, A. (1998), The evolution of aircraft emissions in the stratosphere, *Geophys. Res. Lett.*, *25*(12), 2129–2132.

Gettelman, A., and S. L. Baughcum (1999), Direct deposition of subsonic aircraft emissions into the stratosphere, *J. Geophys. Res.*, *104*, 8317–8327.

Gettelman, A., and A. H. Sobel (2000), Direct diagnoses of stratosphere-troposphere exchange, *J. Atmos. Sci.*, *57*(1), 3–15.

Grise, K. M., D. W. J. Thompson, and T. Birner (2010), A global survey of static stability in the stratosphere and upper troposphere, *J. Atmos. Sci.*, *23*, 2275–2292.

Haynes, P. H., and E. Shuckburgh (2000), Effective diffusivity as a diagnostic of atmospheric transport: 2. Troposphere and lower stratosphere, *J. Geophys. Res.*, *105*, 22,795–22,810.

Haynes, P. H., C. J. Marks, M. E. McIntyre, T. G. Shepherd, and K. P. Shine (1991), On the "downward control" of extratropical diabatic circulations by eddy-induced mean zonal forces, *J. Atmos. Sci.*, *48*(4), 651–678.

Hegglin, M. I., C. D. Boone, G. L. Manney, and K. A. Walker (2009), A global view of the extratropical tropopause transition layer from atmospheric chemistry experiment fourier transform spectrometer O_3, H_2O, and CO, *J. Geophys. Res.*, *114*, D00B11, doi:10.1029/2008JD009984.

Herndon, S. C., et al. (2004), NO and NO_2 emission ratios measured from in-use commercial aircraft during taxi and takeoff, *Environ. Sci. Technol.*, *38*, 6078–6084.

Holton, J. R., P. H. Haynes, M. E. McIntyre, A. R. Douglass, R. B. Rood, and L. Pfister (1995), Stratosphere-troposphere exchange, *Rev. Geophys.*, *33*(4), 403–439.

Hoor, P., H. Wernli, and M. I. Hegglin (2010), Transport timescales and tracer properties in the extratropical UTLS, *Atmos. Chem. Phys.*, *10*, 12,953–12,991.

Huber, M., J. C. McWilliams, and M. Ghil (2000), A climatology of turbulent dispersion in the troposphere, *J. Atmos. Sci.*, *58*, 2377–2394.

Jacobson, M. Z. (2008), Effects of wind-powered hyrdogen fuel cell vehicles on stratospheric ozone and global climate, *Geophys. Res. Lett.*, *35*, L19803, doi:10.1029/2008GL035102.

Jacobson, M. Z. (2010), Short-term effects of controlling fossil-fuel soot, biofuel soot and gases, and methane on climate, Arctic ice, and air pollution health, *J. Geophys. Res.*, *115*, D14209, doi:10.1029/2009JD013795.

Jacobson, M. Z., J. T. Wilkerson, A. D. Naiman, and S. K. Lele (2011), The effects of aircraft on climate and pollution. Part I: Numerical methods for treating the subgrid evolution of discrete size- and composition-resolved contrails from all commercial flights worldwide, *J. Comput. Phys.*, *230*, 5115–5132, doi:10.1016/j.jcp.2011.03.031.

Köhler, M., G. Rädel, O. Dessens, K. Shine, H. Rogers, O. Wild, and J. Pyle (2008), Impact of perturbations to nitrogen dioxide emissions from global aviation, *J. Geophys. Res.*, *113*, D11305, doi:10.1029/2007JD009140.

Kursinski, E. R., et al. (1996), Initial results of radio occultation observations of Earth's atmosphere using the global positioning system, *Science*, *271*, 1107–1110.

Lee, D. S., D. W. Fahey, P. M. Forster, P. J. Newton, R. C. N. Wit, L. L. Lim, B. Owen, and R. Sausen (2009), Aviation and global climate change in the 21st century, *Atmos. Environ.*, *43*, 3520–3537.

Liang, Q., A. R. Douglass, B. N. Duncan, R. S. Stolarski, and J. C. Witte (2009), The governing processes and timescales of stratosphere-to-troposphere transport and its contribution to ozone in the Arctic troposphere, *Atmos. Chem. Phys.*, *9*, 3011–3025.

Marshall, J., and R. A. Plumb (2008), *Atmosphere, Ocean and Climate Dynamics: An Introductory Text*, Elsevier Acad., New York.

Mazraati, M. (2010), World aviation fuel demand outlook, *OPEC Energy Rev.*, *34*(1), 42–72.

Mellor, G. L., and T. Yamada (1982), Development of a turbulence closure model for geophysical fluid problems, *Rev. Geophys. Space Phys.*, *20*, 851–873.

Olsen, E., et al. (2007), AIRS/AMSU/HSB version 5 CalVal status summary, *Tech. Rep.*, NASA Jet Propulsion Lab., Pasadena, Calif.

Pan, L. L., W. J. Randel, B. L. Gary, M. J. Mahoney, and E. J. Hintsa (2004), Definitions and sharpness of the extratropical tropopause: A trace gas perspective, *J. Geophys. Res.*, *109*, D23103, doi:10.1029/2004JD004982.

Parkinsin, C., et al. (2003), Aqua: An Earth-observing satellite mission to examine water and other climate variables, *IEEE Trans. Geosci. Remote Sens.*, *41*(2), 173–183.

Pierrehumbert, R. T., and H. Yang (1992), Global chaotic mixing on isentropic surfaces, *J. Atmos. Sci.*, *50*(15), 2462–2480.

Roeckner, E., et al. (2010), Sensitivity of simulated climate to horizontal and vertical resolution in the ECHAM5 atmosphere model, *J. Clim.*, *19*, 3771–3790.

Roof, C., et al. (2007), Aviation environmental design tool (AEDT) system architecture, *FAA Doc. AEDT-AD-01*, Fed. Aviation Admin., Washington, D. C.

Schulz, M., et al. (2006), Radiative forcing by aerosols as derived from the AEROCOM present-day and pre-industrial simulations, *Atmos. Chem. Phys.*, *6*, 5225–5246.

Seinfeld, J. H., and S. N. Pandis (1998), *Atmospheric Chemistry and Physics: From Air Pollution to Climate Change*, 74 pp., Wiley, New York.

Shapiro, M. A. (1980), Turbulent mixing within tropopause folds as a mechanism for the exchange of chemical constituents between the stratosphere and the troposphere, *J. Atmos. Sci.*, *37*, 994–1004.

Stevenson, D. S., et al. (2006), Multimodel ensemble simulations of present-day and near-future tropospheric ozone, *J. Geophys. Res.*, *111*, D08301, doi:10.1029/2005JD006338.

Stohl, A., et al. (2003a), Stratosphere-troposphere exchange: A review, and what we have learned from staccato, *J. Geophys. Res.*, *108*(D12), 8516, doi:10.1029/2002JD002490.

Stohl, A., H. Wernli, M. Bourqui, C. Forster, M. A. Linger, P. Seibert, and M. Sprenger (2003b), A new perspective of stratosphere-troposphere exchange, *Bull. Am. Meteorol. Soc.*, *84*, 1565–1573.

Tarrason, L., J. Eiof Jonson, T. K. Berntsen, and K. Rypdal (2004), Study on air quality impacts of non-LTO emissions from aviation, *Tech. Rep. 3*, Rep. to the Eur. Comm. under contract B4-3040/2002/343093/MAR/C1, Norw. Meteorol. Inst., Oslo.

Unal, A., Y. Hu, M. E. Chang, M. T. Odman, and G. R. Armistead (2005), Airport related emissions and impacts on air quality: Application to the Atlanta international airport, *Atmos. Environ.*, *39*, 5787–5798.

Vallis, G. (2006), *Atmospheric and Oceanic Fluid Dynamics: Fundamentals and Large-Scale Circulation*, 4th ed., Cambridge Univ. Press, New York.

Walcek, C. J. (2000), Minor flux adjustment near mixing ratio extremes for simplified yet highly accurate monotonic calculation of tracer advection, *J. Geophys. Res.*, *105*, 9335–9348.

Wickert, J., et al. (2001), Atmosphere sounding by GPS radio occultation: First results from CHAMP, *Geophys. Res. Lett.*, *28*, 3263–3266.

Wilkerson, J. T., M. Z. Jacobson, A. Malwitz, S. Balasubramanian, R. Wayson, G. Fleming, A. D. Naiman, and S. K. Lele (2010), Analysis of emission data from global commercial aviation: 2004 and 2006, *Atmos. Chem. Phys.*, *10*, 6391–6408.

Zhang, Y. (2008), Online-coupled meteorological and chemistry models: History, current status, and outlook, *Atmos. Chem. Phys.*, *8*, 2895–2932.

M. Z. Jacobson, D. B. Whitt, and J. T. Wilkerson, Department of Civil and Environmental Engineering, Stanford University, 473 Via Ortega, Rm. M-26, Stanford, CA 94305, USA. (dwhitt@stanford.edu)

S. K. Lele and A. D. Naiman, Department of Aeronautics and Astronautics, Stanford University, 496 Lomita Mall, Rm. 267, Stanford, CA 94305, USA.